Geophys. Astrophys. Fluid Dynamics, Vol. 76, pp. 1–27
Reprints available directly from the publisher
Photocopying permitted by license only

ROTATING HYDRAULIC MODELS OF FRONTS AT THE CONTINENTAL SHELF BREAK AND IN CIRCULAR EDDIES

J. A. WHITEHEAD

Woods Hole, MA 02543

Department of Physical Oceanography, Woods Hole Oceanographic Institution, Woods Hole, MA 02543. U.S.A.

RYUJI KIMURA

Division of Marine Meteorology, Ocean Research Institute, University of Tokyo, 1-15-1 Minamidai, Nakano-ku Tokyo, Japan 164

(*Received 11 February 1994; in final form 10 May 1994*)

We explore a mechanism that uses inertia to produce flux across a geostrophic front that separates two fluids of differing density in a rotating fluid. We ask "when the front is forced to be narrower than the Rossby Radius R so the full Rossby adjustment cannot be reached, will fluid continue to flow in a cross-frontal direction and if so at what rate?" A simplified model is considered with flow in a submerged horizontal slot between two very deep basins containing motionless water. The inviscid rotating nonlinear equations for exchange flow are solved for two configurations: The first has Cartesian coordinates and the slot is infinitely wide but of length l in the cross-frontal direction. Volume flux decreases with increasing rotation rate and ultimately goes to zero when Rossby radius $R = l$. The second case has cylindrical coordinates. Flux also decreases with increasing rotation rate and goes to zero when the difference between radii equals $2\sqrt{2}\gamma R/(1+\gamma)\sqrt{1+\gamma^2}$ where γ is the outer radius divided by the inner radius. This may be important for eddies or cyclones in the ocean or atmosphere. An experiment had an electrically heated cylindrical chamber separated from an outer cold water basin by a horizontal annular slot. The temperature difference between the two chambers was measured for known heat flux and various rotation rates. As rotation increases from zero, temperature difference increases. Volume flux must correspondingly decrease. Above a critical rotation rate a flow with eddies emerges (probably from baroclinic instability) with smaller temperature difference (thus greater volume flux) than predicted.

KEY WORDS: Hydraulic control, continental shelves, fronts.

1. INTRODUCTION

Fronts in the atmosphere or the ocean separate fluids of different density. The principal flow is along the front. Cross frontal transport is frequently important, but small and difficult to both measure and estimate. Fronts in the ocean are frequently found near topographic features, one of the largest being the edge of a continental shelf. Here, fronts often serve as barriers between coastal water and deep sea water (Flagg and Beardsley 1978; Walsh *et al.*, 1988; Chao, 1990; Gawarkiewicz 1991; Gawarkiewicz and Chapman 1992; Vincent *et al.*, 1993), since in many cases water on the continental shelf has distinctly different temperature, salinity, (thence usually density), dissolved

materials and suspended particles than nearby deep ocean water at the same depth. Time averaged components of the currents generally tend to follow bathymetric contours, so that the front appears to correlate with the shelf break and "trap" or guide the water along the shelf. This happens in spite of the fact that tides, winds, waves, eddies, and meanders of fronts lead to large, temporary across-shelf velocities.

The small transport across shelf edge fronts is important (Walsh, *et al.*, 1988). Unfortunately the volumetric flux and transport of heat, salt or tracers across fronts from shelf to deep ocean is poorly measured and understood. To determine transport, the data of velocity and heat, salt or tracer concentration must be averaged over long times or long distances. In this case, unfortunately, the state of the shelf may change with the seasons and not remain in one stage long enough for oceanographers to acquire significant data.

Cross-frontal flux must be produced by effects from either friction, mixing, or inertia. The role of friction and mixing has been explored in a number of cases. Stommel and Leetmaa, (1972) for instance, found theoretical solutions to a problem with a mean cross-shelf density gradient, in which earth rotation, surface stress and the effect of viscosity and diffusivity were included. The flux produced by the flow in the Ekman layers was an essential ingredient in the cross-shelf transport. Csanady (1984) has also utilized parameterized stress in Ekman layers to produce a flux across a front at the edge of the shelf. Hignett, *et al.*, (1981) studied convection from non-uniform bottom heating in a rotating annulus. For small rotation, flow parallel to temperature gradient (hence heat transport) is found only in boundary layers. There is no transfer in the interior, which has a "zonal" thermal wind perpendicular to the temperature gradient. Numerous other analytical and numerical models have produced cross-shelf flux using viscosity to produce cross-shelf or cross-frontal exchange.

The role of inertia to produce cross-front transport is less well explored. There is no doubt that the geostrophic shelf currents can be baroclinically unstable under some circumstances and that inertia plays a role in that instability. Analytical studies of large amplitude eddy transport remain poorly developed. In assorted cases an eddy resolving numerical experiment, which uses for instance the quasi- or semi-geostrophic approximation can be constructed to estimate cross-shelf transport, but the understanding of the transport processes gained from analytical solutions is usually absent.

In an attempt to quantify cross-shelf flux, one of us (Whitehead, 1993) recently conducted measurements of heat flux from shelf to deep water in a laboratory model of a shelf which was cooled from above and adjacent to warm offshore water. A principal barrier to the heat flux appeared to be the front which developed over the shelf break. The front was approximately a Rossby Radius of deformation in width, but it was not clear whether the measured flux relationship came from an eddy flux or from Ekman layer processes (or both).

The presence of the front and its unknown role in the transport has motivated this study, which explores the possibility that inertia leads to a cross shelf flux through a mechanism different from baroclinic instability. The mechanism relies on the fact that inertia is involved in the Rossby adjustment problem which involves cross frontal transport during the adjustment. In this problem, two motionless fluids in a field of gravity are initially separated by a vertical barrier (Figure 1a). When the barrier is removed, an interface between the two fluids changes due to gravitational slumping

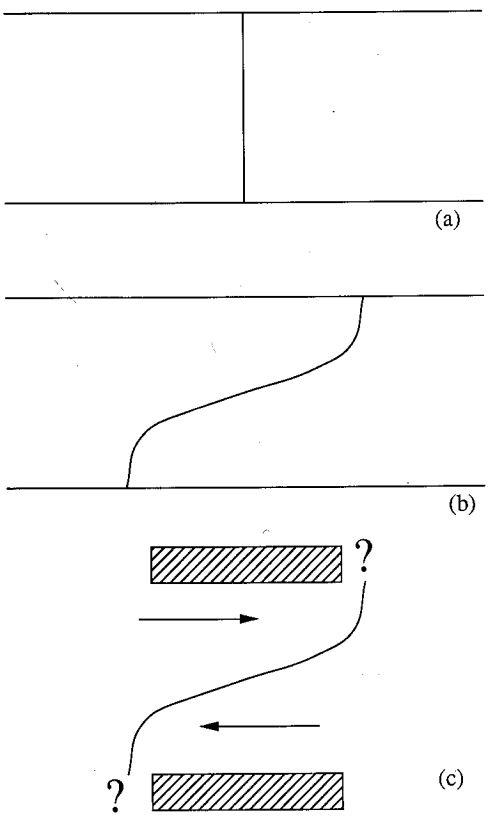

Figure 1 Sketch of the idealized thought experiment. (a) Initially a barrier separates regions of differing density. (b) After the barrier is released, the fluid experiences the Rossby adjustment process and a front forms that is approximately a Rossby radius in width. (c) We inquire here about the flux if the region is narrower than a Rossby radius so the full adjustment cannot take place. In that case, there continues to be a flow along the channel in the adjustment direction.

(which we take to be cross frontal transport), accelerates the fluid, and ultimately produces a sloping front whose width is the well-known Rossby radius of deformation (Figure 1b). At the final stage acceleration and cross frontal transport have ceased, and a steady geostrophic (or in the case of continuous stratification-thermal wind) flow is found. It is often thought that fronts are in this final state, and that they possess little or no cross frontal transport.

Some circumstances may exist where fronts do not reach the full width of the Rossby Radius. Possibly a shelf is too narrow, or possibly boundary layers remove fluid at the edges of the front, for example. In this study we force a front to be narrower than the Rossby radius of deformation. We wonder whether the cross frontal transport continues indefinitely. We therefore ask the question "when the region of adjustment is narrower than the Rossby Radius, so the full Rossby adjustment cannot be reached (Figure 1c), will fluid continue to flow in a cross-frontal direction and if so at what rate?"

Of all past laboratory studies of a fluid flow like this, the annulus experiments are probably those with closest resemblance to the present problem. In these experiments, an annular container of water was heated at one radial wall and cooled at the other. Usually the fluid was thermally insulated along the top and bottom. It was found that for very low rates of rotation the flow developed a Hadley cell, with rising at the warm wall and sinking at the cold wall. In between there was an exchange flow similar to the flow we describe here. The flows and structure of the Hadley circulation, and the influence of rotation on that circulation was analyzed by Robinson (1959), and Barcilon (1962). In contrast to the present study, the interior flows were set up by the convergence and divergence in both thermal and viscous (Ekman) boundary layers. At small rotation rates the flow was found to be symmetric and at greater rotation rates the flow developed baroclinic instabilities. Barcilon (1964) showed that the basic flow had more potential energy available than would be dissipated by friction and thus showed how the annular flows become unstable. The instabilities were manifest by the formation of eddies in some cases and a meandering of a jet from the inner to the outer wall in other cases. Flow regimes were described as a function of the dimensionless parameters by Fowlis and Hide (1965) and heat flux was measured by Bowden and Eden (1965). Flow regimes and heat flow for the case of axisymmetric heating from below were reported by Hignett, *et al.* (1981).

2. THEORY OF WIDE ROTATING LOCK-EXCHANGE FLOW

To study the effect of rotation on inviscid cross-frontal flux in as uncomplicated a system as possible, consider first a simplified model of a uniformly rotating continental shelf region. A reservoir of still water in the deep ocean is separated by a planar shelf of uniform depth from a reservoir of still water of different density near the coast. We ask "what is the rate of exchange between the two regions?" In order to be sure that the upstream fluids remain motionless even if there is exchange flow between ocean and coastal region, two very deep basins instead of shallow layers containing motionless waters of differing densities will be considered. They are separated by a vertical wall except at mid-depth where there is a horizontal slot of depth h, cross-shelf length l and of infinite width (see Figure 2). At some previous time the slot had been opened, the interface between the two fluids slumped from gravity, and fluid started flowing back and forth between the basins (as in the Rossby adjustment problem). A steady exchange flow is reached where low density fluid flows along the top of the slot from basin 1 to basin 2 and a counterflow flows along the bottom of the slot from basin 2 to basin 1. It will be assumed that the reservoirs on either side of the slot are large but finite and that fluid is not being added to either basin from the outside. Thus when enough time has elapsed for pressures p_1 and p_2 to adjust, the volume flux from basin 1 to basin 2 becomes the same as the flux from basin 2 to basin 1. We seek to calculate Q, the volume flux per unit slot width for the case of inviscid fluids.

It is necessary to position the slot at mid-depth to remove fluid from the region next to the slot that is receiving the lighter fluid. If the slot were at the surface the low density fluid would continue to pile up next to the slot and block the removal of additional fluid. The slot at mid-depth causes the coastal front analogy to break down to some

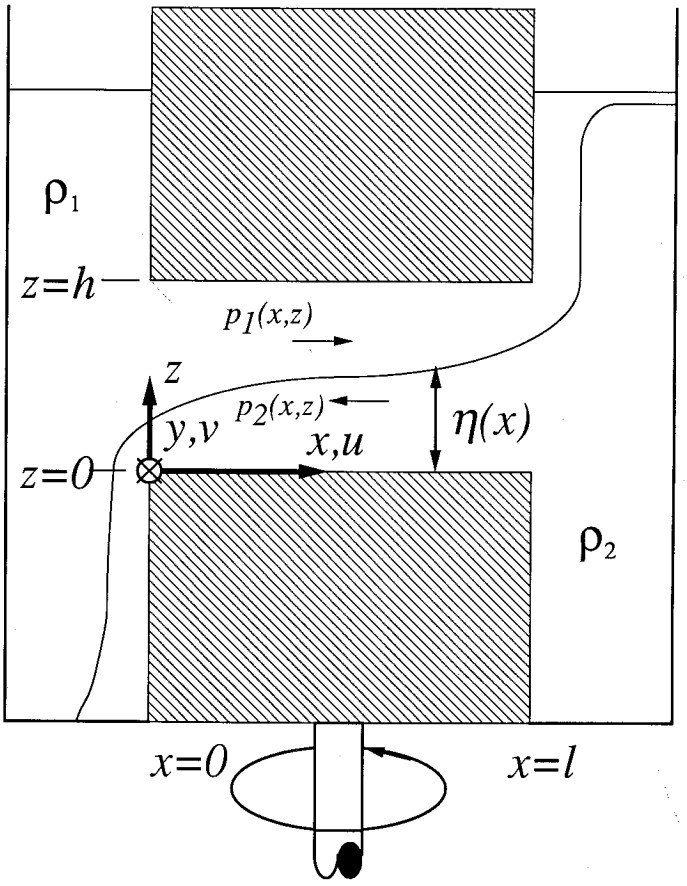

Figure 2 Sketch of the idealized problem that is studied here. A horizontal slot of length l in a rotating coordinate system separates two reservoirs with water of differing density. The slot is infinitely wide in the direction out of the page.

extent because the continental shelf is at the surface. However, in the ocean possibly mixed layers or offshore currents could transport low density fluid away from the edge of the shelf break and make the application more valid than is apparent at first glance.

In either layer, the steady inviscid Boussinesq shallow water equations of motion are

$$u_n\frac{\partial u_n}{\partial x}+v_n\frac{\partial u_n}{\partial y}-fv_n=-\frac{1}{\rho}\frac{\partial p_n}{\partial x}, \tag{1}$$

$$u_n\frac{\partial v_n}{\partial x}+v_n\frac{\partial v_n}{\partial y}+fu_n=-\frac{1}{\rho}\frac{\partial p_n}{\partial y}, \tag{2}$$

$$0=-\frac{1}{\rho_n}\frac{\partial p_n}{\partial z}-g. \tag{3}$$

The coordinates and their origins are shown in Figure 2. The velocities u and v are in the cross-slot (x) and along slot (y) direction, respectively. The subscript $n = 1, 2$ refers to the top (lower density) and bottom (higher density) fluid, respectively. Since the slot is infinitely wide, the y derivative is zero so that

$$u_n \frac{\partial u_n}{\partial x} - f v_n = -\frac{1}{\rho}\frac{\partial p_n}{\partial x}, \tag{4}$$

$$u_n \frac{\partial v_n}{\partial x} + f u_n = 0. \tag{5}$$

If $u_n = 0$, flow is geostrophic and there is no cross frontal flux. If $u_n \neq 0$, there is a flux. We seek solutions to that case. Equation (5) implies

$$\frac{\partial v_n}{\partial x} = -f, \tag{6}$$

which integrates to

$$v_n = -fx + v_{no}. \tag{7}$$

The constant of integration for layer n is the velocity v_{no} at $x = 0$. In addition, using (6) in (4),

$$u_n \frac{\partial u_n}{\partial x} + v_n \frac{\partial v_n}{\partial x} = -\frac{1}{\rho}\frac{\partial p_n}{\partial x}, \tag{8}$$

which integrates to Bernoulli's equation

$$\tfrac{1}{2}(u_n^2 + v_n^2) + \frac{p_n(x, z)}{\rho} = \frac{p_n((-1^n)\infty, z)}{\rho}, \tag{9}$$

where it has been assumed that fluid is motionless i.e. $u_n = v_n = 0$ in the reservoirs. At $z = h$ in layer 1,

$$\tfrac{1}{2}(u_1^2 + v_1^2) + \frac{p_1(x, h)}{\rho} = \frac{p_1(-\infty, h)}{\rho} \tag{10}$$

and at $z = 0$ in layer 2,

$$\tfrac{1}{2}(u_2^2 + v_2^2) + \frac{p_2(x, 0)}{\rho} = \frac{p_2(\infty, 0)}{\rho}. \tag{11}$$

The hydrostatic equation (3) is integrated vertically in the slot to give

$$p_1(x,h) + \rho_1 g(h-\eta) + \rho_2 g\eta = p_2(x,0), \tag{12}$$

where $\eta(x)$ is thickness of layer 2 in the slot. Subtract (11) from (10) and use (12) along with the relation $p_2(\infty,0) = p_2(\infty,h) + \rho_2 gh$ to get

$$\tfrac{1}{2}\rho(u_1^2 + v_1^2 - u_2^2 - v_2^2) + (\rho_2 - \rho_1)g(h-\eta) = p_1(-\infty,h) - p_2(\infty,h). \tag{13}$$

Now since $v_1 = 0$ at $x = 0$ has been prescribed, equation (7) gives

$$v_1 = -fx. \tag{14}$$

Since $v_2 = 0$ at $x = l$, equation (7) also gives

$$v_2 = -f(x-l), \tag{15}$$

so (13) becomes

$$\tfrac{1}{2}\rho[u_1^2 - u_2^2 + f^2x^2 - f^2(x-l)^2] + \Delta\rho g(h-\eta) = \Delta p, \tag{16}$$

where $\Delta\rho = \rho_2 - \rho_1$, $\Delta p = p_1(-\infty,h) - p_2(\infty,h)$. For simplicity assume symmetry between flow going to the left and right so that at $x = l/2$, $\eta = h/2$, $u_1 = -u_2$ and $\Delta\rho gh/2 = \Delta p$. The more general case without symmetry is solved in the next section where it is shown that the symmetric flow has greatest volume flux Q per unit width. Finally let $Q = u_1(h-\eta) = -u_2\eta$, then define $\delta(x) = h/2 - \eta(x)$ and $g' = g\Delta\rho/\rho$. Equation (16) becomes

$$\frac{1}{2}Q^2\left[\frac{1}{(\frac{1}{2}h+\delta)^2} - \frac{1}{(\frac{1}{2}h-\delta)^2}\right] - \frac{f^2(l^2-2xl)}{2} + g'\delta = 0. \tag{17}$$

To investigate properties of this solution, it is useful to define

$$Q' = \frac{4Q}{\sqrt{g'h^3}},$$

transform to $x' = (2x/l) - 1$ and write (17) in the form

$$\frac{Q'^2}{4}\left[\frac{1}{(1-\varepsilon)^2} - \frac{1}{(1+\varepsilon)^2}\right] = \varepsilon + \alpha^2 x', \tag{18}$$

where $\alpha^2 = f^2l^2/g'h$ and $\varepsilon(x') = 2\delta/h$. The variable α is the length of the slot divided by the Rossby Radius R and is a measure of the strength of rotation. The variable $\varepsilon(x')$ is a freely adjustable parameter corresponding to deviation of the interface from the midplane of the slot.

Let us investigate the effects of different values of Q' x' and α as a function of ε. The functions corresponding to the left and right hand sides of (18) as a function of ε are drawn in Figure 3a, c, and e. For fixed Q' and α the solution is the intersection of a curve corresponding to the left hand side of (18) and a series of straight lines with unity slope

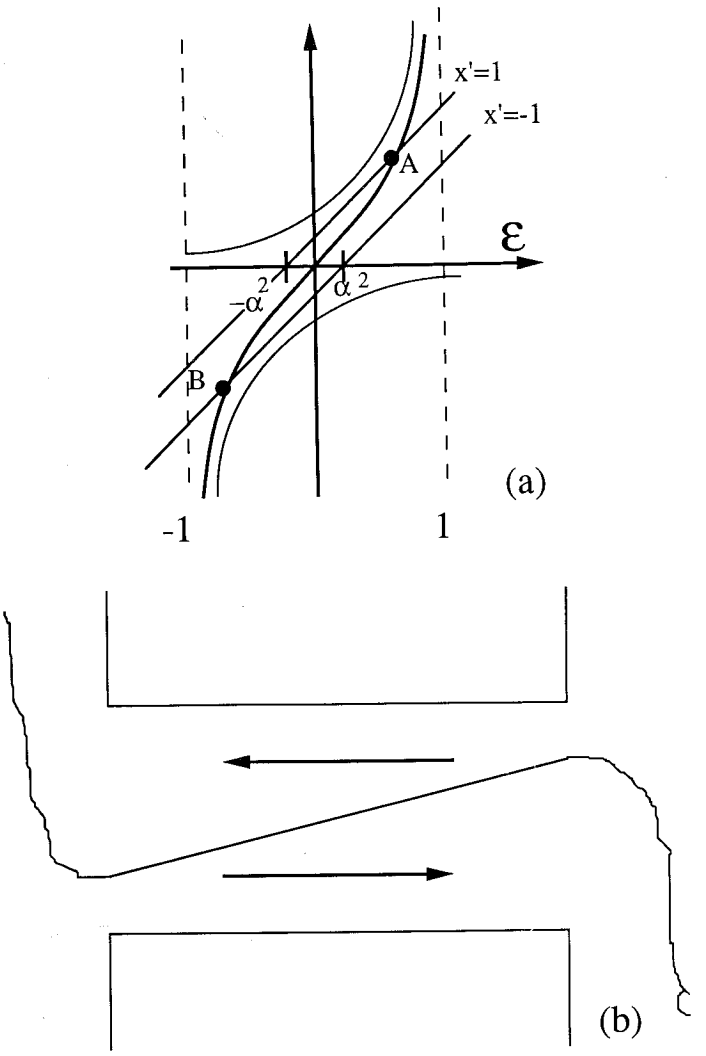

Figure 3 Sketch of the different solutions of equation (18). (a) Generating hyperbolas, curve for $Q' > 1$, and two end lines corresponding to the end points of the flow at $|x'| = 1$. A smooth solution extends from A to B. (b) Sketch of the interface between the two fluids along the slot. (c) Curve for $Q' = Q'_c$. The curve touches the end lines in points C′ and D′ and a smooth solution extends between these two points. This critical flow is expected to be physically realized. There are also nonsymmetric solutions from C to C′ and D to D′. (d) Sketch of the interface for the critical flow solution. The light curve is the extension of the solution from C′ to C and D′ to D. The heavy curve is the expected outflow beyond the slot. (e) For $Q' > Q'_c$ the solution extends from A to A′ and then must jump to B′ before arriving at B. This violates the assumption of symmetry.

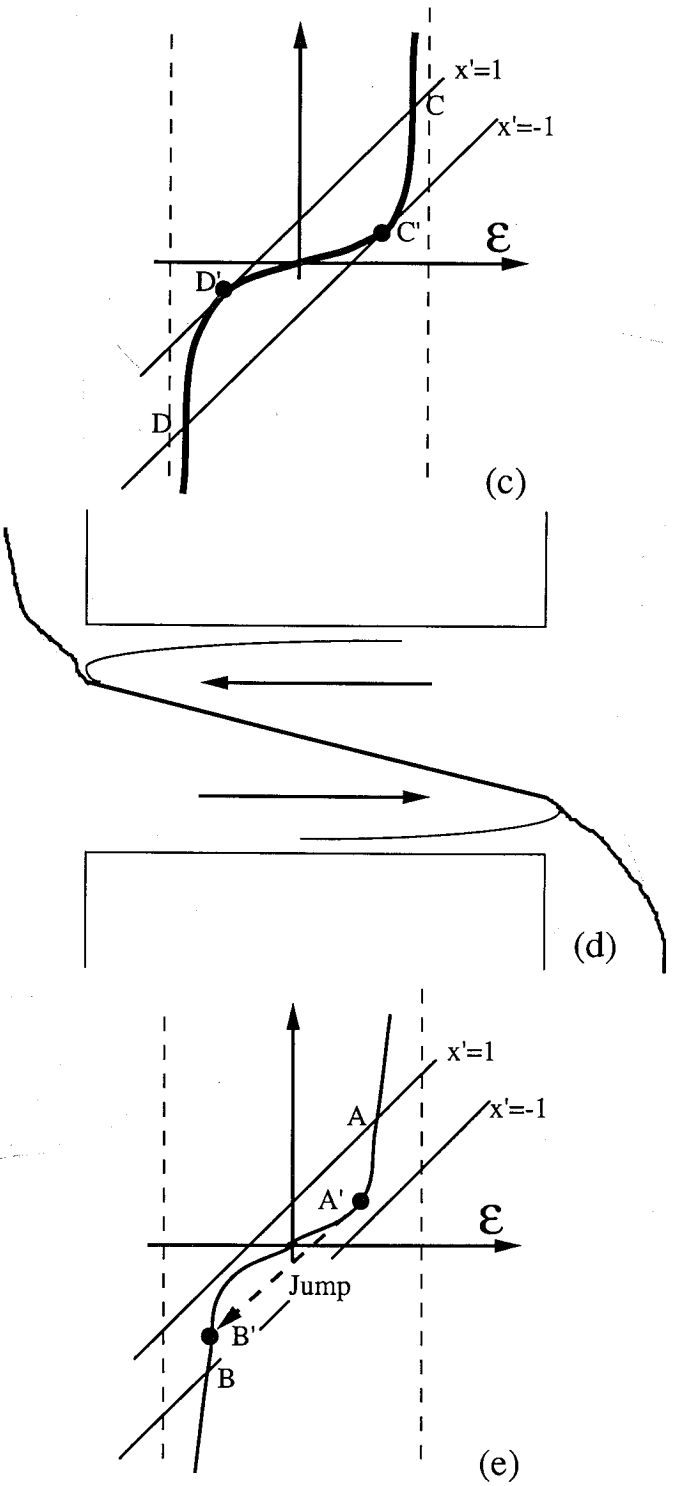

Figure 3 (*Continued.*)

that correspond to different values of x' from the right hand side. It is helpful to note that the curve corresponding to the left hand side is the sum of two hyperbolas (Figure 3a) and this ensures that $|\varepsilon| < 1$.

First note that if $Q' > 1$ (Figure 3a), the slope of the curve is greater than 1 everywhere but each member of the group of straight lines has unity slope. Thus each line intersects the curve at only one point so there is only one value of ε for each x'. The solution extends continuously from point A (where the line corresponding to $x' = 1$ intersects the curve) to point B (where the line corresponding to $x' = -1$ intersects the curve). The curve of ε versus x' (Figure 3b) is typical of supercritical flows, with the fluid flowing from a thin part of the layer to a thicker part. The flows shown in Figure 3a will be called supercritical, even though they have not been shown here to possess Froude number greater than one.

For $Q' < 1$ (Figure 3c, and e), the slope of the curve from the left hand side is less than one near $\varepsilon = 0$ and the solution becomes more complicated. Only when Q' becomes small enough can a smooth solution connect the two ends of the channel for fixed value of α (i.e. fixed ratio of channel length to Rossby radius of deformation). The curve for which this happens is shown in Figure 3c. It is marked by the letters C′ and D′ which are the end points for the smooth solution. This appears to be the solution that would be physically realized. It exists for only one value of Q' which will be called Q'_c (a critical value). It is also the largest possible value of Q' for $Q' < 1$ with continuous flow between the endpoints. The slope of the curve is 1 where it intersects the two lines (whose slopes are also 1), so that the change of ε with x' is infinite at $x' = \pm 1$. Whitehead and Porter (1977) found the same results for unidirectional axisymmetric flow. They asserted that this corresponds to a critical control condition, since a slightly wider slot requires that the volume flux must change.

At larger values of $|\varepsilon|$ lie two more trajectories which can be followed from C′ to C or D′ to D. The value of $|\varepsilon|$ increases toward a value close to $|\varepsilon| = 1$. This solution branch should also be rejected as it violates our assumption of symmetry between left and right hand flow directions (these branches are shown as thin lines in Figure 3d). They represent solutions in which flow in one layer is rapid and flow in the other layer is slow.

For a given value of α, and $1 > Q' > Q'_c$, solutions do exist but they are asymmetric and discontinuous as shown in Figure 3e. A solution follows the curve from $x' = 1$ downward from point A at $\varepsilon = \alpha^2$ to a point A′ where the curve has a slope of one. Beyond that point if the curve is followed the interface returns to larger values of x'. It is unphysical to follow this bend, as it corresponds to the interface doubling back toward larger x'. To proceed to smaller x', the solution must jump to point B′, then move smoothly to B. This violates our assumption of symmetry and we consider such solutions ill behaved. Moreover, at the jump point the slope of the curve is one so the change of ε with x' is infinite. Thus this is a shock.

There are trajectories $Q' < Q'_c$ and these represent symmetric subcritical flows. Such flows would be physically realized if the upstream and downstream basins each contained both fluids with interfaces at depths close to the depth of the slot. In such a case the flows are not hydraulically controlled by the slot.

Proceeding, equation (18) at $x' = 1$ can be rearranged to become

$$Q' = \left[\left(1 - \frac{\alpha^2}{\varepsilon}\right)(1-\varepsilon^2)^2\right]^{1/2}. \tag{19}$$

This makes it easy to see that ε is negative for $Q' > 1$. In addition Q' is unbounded as negative ε approaches 0. This feature makes the supercritical solutions appear to be very unphysical, so the subcritical solution appears to be preferable. For these $0 < \varepsilon < 1$, and the equation shows that a real solution is not possible for $\alpha > 1$. Also, in general the term $1 - \alpha^2/\varepsilon$ is negative for $0 < \varepsilon < \alpha^2$ in which case no flux is possible and flux is zero at $\varepsilon = \alpha^2$. For $\varepsilon > \alpha^2$, flux increases rapidly with ε but then it must decrease to zero for $\varepsilon = 1$, so there is a maximum value of flux in the range $\alpha^2 < \varepsilon < 1$.

The dependence of Q' on ε for 7 values of α^2 is shown in Figure 4a. When α^2 approaches zero, flux is maximum for $\varepsilon \cong \alpha^{2/3}$ and takes the value $Q' = 1$ which is the well known value for the non-rotating exchange problem (Yih, 1980, p 206).

Since ε is a free parameter, its value that gives maximum flux will be selected if the flow is critically controlled. We now assume that the flow is critically controlled, and seek an expression for flux. Setting $\partial Q'/\partial\varepsilon = 0$, we find

$$\varepsilon_c^3 - \tfrac{3}{4}\alpha^2\varepsilon_c^2 - \tfrac{1}{4}\alpha^2 = 0, \tag{20}$$

where subscript c denotes the critical value. It is easy to calculate the value of α for given ε_c, it is

$$\alpha^2 = 4\varepsilon_c^3/(3\varepsilon_c^2 + 1). \tag{21}$$

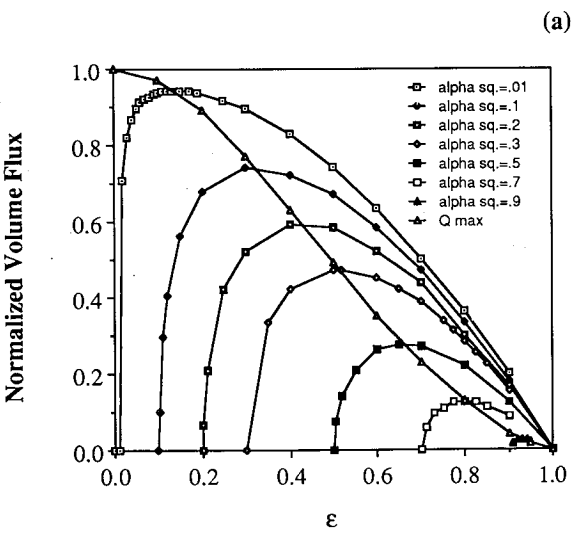

Figure 4 (a) Normalized volume flux Q' as a function of scaled interface displacement ε at the edge of the slot for different rotation rates. The trajectory of the maximum of the seven curves is also shown. (b) Values of ε versus α^2 for maximum flux. (c) Maximum normalized volume flux Q'_c versus α^2.

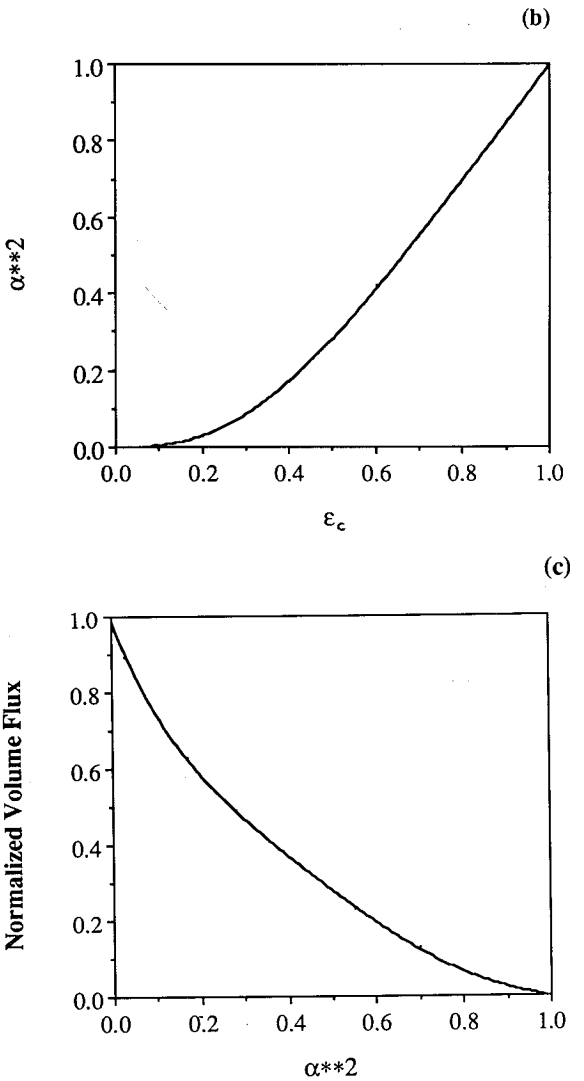

Figure 4 (*Continued.*)

This relation is drawn in Figure 4b. It can now be inserted into (19) to give

$$Q_c' = [(1 - \varepsilon_c^2)^3/(3\varepsilon_c^2 + 1)]^{1/2}. \tag{22}$$

This is also included in Figure 4a. Figure 4c shows Q_c' versus α^2. This is most simply calculated by using (21) and (22) and varying ε_c between 0 and 1.

We see, starting from the value $\varepsilon_c = 0$, that in equation (21), α^2 also starts from 0 and is equal to $4\varepsilon_c^3$ so that for $\alpha^2 \ll 1$

$$Q_c' \cong 1 - \frac{3}{2}\varepsilon_c^2 = 1 - \frac{3}{2}\left[\frac{\alpha}{2}\right]^{4/3}. \tag{23}$$

For $\alpha \cong 1$ there is a large effect of rotation. To solve, let $\alpha^2 = 1 - \xi$, and $\varepsilon = 1 - \mu$ in (19),

$$Q' = \left[\frac{(\xi - \mu)\mu^2(2-\mu)^2}{1-\mu}\right]^{1/2}. \tag{24}$$

Assuming $\mu \ll 1$ and taking the derivative with μ yields $\mu_c = 2\xi/3$, then (24) reduces to

$$Q_c' = \frac{4}{3\sqrt{3}}\xi^{3/2} = \frac{4}{3\sqrt{3}}(1-\alpha^2)^{3/2}. \tag{25}$$

This tells us a very simple fact: The flux is equal to the flux for zero rotation times a term that goes to zero as the length of the slot approaches the Rossby radius of deformation. If slot length equals the Rossby radius a flow similar to the Rossby adjusted flow (but in a Cartesian geometry) exists; it has a front lying in the slot and no fluid travels through the slot. When length is close to the Rossby radius (i.e. for small μ), then (25) has become identical to the equation governing a critical control problem for a rotating one-layer problem (Sambuco and Whitehead, 1976; Whitehead and Porter, 1977). This is because firstly the thickness of the fluid layer μ at the control point is very small compared to the depth of the layer above or below it, and secondly the velocity in the thin fluid layer is much greater than the velocity of the fluid in the other layer.

3. TWO-LAYER EXCHANGE FLOW IN CYLINDRICAL COORDINATES

In hope of formulating a theory applicable to a laboratory experiment, a two-layer flow in an axisymmetric cylindrical geometry is analyzed using approaches that are similar to those used in the preceding section. The results may be interesting in their own right since they could apply to features in the ocean (for instance gulf stream rings or meddies) or atmosphere (cyclones or other mesoscale eddies). A sketch of the geometry is shown in Figure 5. Fluid of density ρ_2 flows inward within a bottom layer from the "outer" radius r_o to the "inner" radius r_i. Fluid of density ρ_1 flows outward in a top layer. The steady axisymmetric horizontal equations of motion are

$$u_n\frac{\partial u_n}{\partial r} - \frac{v_n^2}{r} - fv_n = -\frac{1}{\rho}\frac{\partial p_n}{\partial r}, \tag{26}$$

$$u_n\frac{\partial v_n}{\partial r} + \frac{u_n v_n}{r} + fu_n = 0. \tag{27}$$

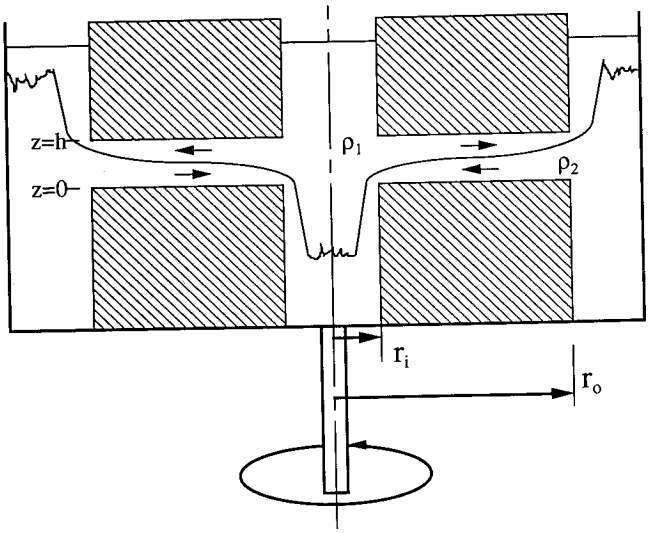

Figure 5 Geometry of the cylindrical problem.

The velocities u and v are now in radial and angular directions, respectively. Since $u_n \neq 0$, equation (27) requires that

$$\frac{\partial v_n}{\partial r} + \frac{v_n}{r} + f = 0, \tag{28}$$

which has a solution

$$v_n = \frac{c_n}{r} - \frac{fr}{2}. \tag{29}$$

Using (28), then (26) integrates at $z = h$ in layer 1 to

$$\tfrac{1}{2}\rho(u_1^2 + v_1^2) + p_1(r, h) = p_1(r_i, h) \tag{30}$$

and at $z = 0$ in layer 2 to

$$\tfrac{1}{2}\rho(u_2^2 + v_2^2) + p_2(r, 0) = p_2(\infty, 0). \tag{31}$$

The hydrostatic equation (3) is the same as before. It is integrated vertically in the slot to give

$$p_1(r, h) + \rho_1 g(h - \eta) + \rho_2 g\eta = p_2(r, 0). \tag{32}$$

Subtract equation (30) from (31) and use (32) plus $p_2(\infty,0)=p_2(\infty,h)+\rho_2 gh$ to get

$$\tfrac{1}{2}\rho(u_1^2+v_1^2-u_2^2-v_2^2)+(\rho_2-\rho_1)g(h-\eta)=p_1(r_i,h)-p_2(\infty,h). \tag{33}$$

Equation (29) with the assumption that upstream fluid is motionless in layer 2 so that $v_2=0$ at $r=r_o$ is

$$v_2=\frac{fr_o^2}{2r}-\frac{fr}{2} \tag{34}$$

and $v_1=0$ at $r=r_i$ so

$$v_1=\frac{fr_i^2}{2r}-\frac{fr}{2}. \tag{35}$$

Equation (33) becomes

$$\tfrac{1}{2}\rho\left[(u_1^2-u_2^2)+\left(\frac{fr_i^2}{2r}-\frac{fr}{2}\right)^2-\left(\frac{fr_o^2}{2r}-\frac{fr}{2}\right)^2\right]+\Delta\rho g(h-\eta)=\Delta p. \tag{36}$$

As before, $\Delta\rho=\rho_2-\rho_1$ and $\Delta p=p_1(r_i,h)-p_2(\infty,h)$. Finally assume that volume flux F in through the bottom layer equals volume flux out through the top layer. To picture a situation that leads to this case, assume that the lower fluid flows into the region where $r<r_i$, it is heated there, mixed and then flows out in layer 1. Define $F=2\pi u_1\, r(\frac{1}{2}h+\delta)=2\pi u_2 r(\frac{1}{2}h-\delta)$ where $\eta+\delta=\frac{1}{2}h$. Equation (36) becomes

$$\frac{F^2}{8\pi^2}\left[\frac{1}{r^2(\frac{1}{2}h+\delta)^2}-\frac{1}{r^2(\frac{1}{2}h-\delta)^2}\right]+\frac{f^2}{8}\left[\frac{r_i^4-r_o^4}{r^2}-2(r_i^2-r_o^2)\right]+g'(\tfrac{1}{2}h+\delta)=\frac{\Delta p}{\rho}, \tag{37}$$

where $g'=g\Delta\rho/\rho$. In the preceding Cartesian case, Δp was eliminated with a symmetry assumption. It is not possible to invoke symmetry here. Instead, to eliminate Δp, equation (37) is first applied at r_i then at r_o and the former is subtracted from the latter. The results can be rearranged to become

$$\frac{F^2}{2\pi^2h^2r_i^2}\left[\frac{4\varepsilon_o}{\gamma^2(1-\varepsilon_o^2)^2}-\frac{4\varepsilon_i}{(1-\varepsilon_i^2)^2}\right]-\frac{f^2r_i^2}{8\gamma^2}(1-\gamma^4)(1-\gamma^2)-\frac{g'h}{2}(\varepsilon_o-\varepsilon_i)=0, \tag{38}$$

where $\gamma=r_o/r_i$, $\varepsilon_i=2\delta_i/h$, and $\varepsilon_o=2\delta_o/h$. With further rearranging, volume flux is

$$F=\frac{2\pi r_i\sqrt{g'h^3}}{4}\left\{\frac{\left[\varepsilon_i-\varepsilon_o-\dfrac{\alpha_r^2}{4\gamma^2}(1-\gamma^4)(1-\gamma^2)\right]\gamma^2(1-\varepsilon_i^2)^2(1-\varepsilon_o^2)^2}{\gamma^2\varepsilon_i(1-\varepsilon_o^2)^2-\varepsilon_o(1-\varepsilon_i^2)^2}\right\}^{1/2}, \tag{39}$$

where $\alpha_r^2=f^2r_i^2/g'h$. As in the Cartesian case, flux is scaled by the term outside the brackets which we presume is the solution of the non-rotating problem. The flux also depends on the following other parameters that are inside the brackets: First is the

dimensionless number α_r, which is a dynamic variable that expresses the strength of the rotation. It has a direct counterpart in the Cartesian problem, although we will find that values of this parameter which govern the volume flux may differ from those in the Cartesian solution. Second is the dimensionless number γ, which is the ratio of the outer and inner radii. It is a geometric variable and has no counterpart in the Cartesian solution. The Cartesian results are recovered in the limit when γ gets close to 1. The other two parameters $\varepsilon_{i,o}$ represent the deviation of depth of the fluid from mid-depth at the inner and outer radius, respectively and can be freely varied from -1 to 1. It is usually thought that a critically controlled solution will have the maximum value of Q for all possible values of these two parameters.

It is easy to show that the Cartesian limit [equation (19)] can be recovered from (39) when γ is slightly greater than one. For other values of γ simple analytical solutions have not been found, but numerical solutions for any value of γ and α_r are readily obtained using standard computers and programs (we used Matlab). Illustrations of the results are shown in Figures 6–9. Results for the Cartesian case are almost exactly recovered for $\gamma = 1.01$, $\varepsilon_o = -\varepsilon_i$. Flux per unit length at the inner radius $Q'[=4F/2\pi r_i\sqrt{g'h^3}]$ was calculated using (39) as a function of ε_o for seven values of α_r. The results are shown in Figure 6 and the agreement with Figure 4a for the Cartesian counterpart is closer than the width of the lines.

Of course, this formulation allows ε_i and ε_o to be varied independently. Contour plots of Q' for the full range of ε_o and ε_i with $\gamma = 1.01$ and three values of α_r are shown in Figure 7. These illustrate the manner in which increasing rotation cuts off flux at larger values of both ε_i and ε_o. They also show that for this value of γ the greatest flux is found when $\varepsilon_o = -\varepsilon_i$, so the symmetry assumption used in the previous section is verified.

Larger values of γ reveal some new features that are produced by the cylindrical geometry. Contour plots are shown for the values of $\gamma = 1.1$, 2.0, and 100 in Figure 8. We first describe results for $\alpha_r = 0$ (left) which are functions only of the geometry as quantified by γ.

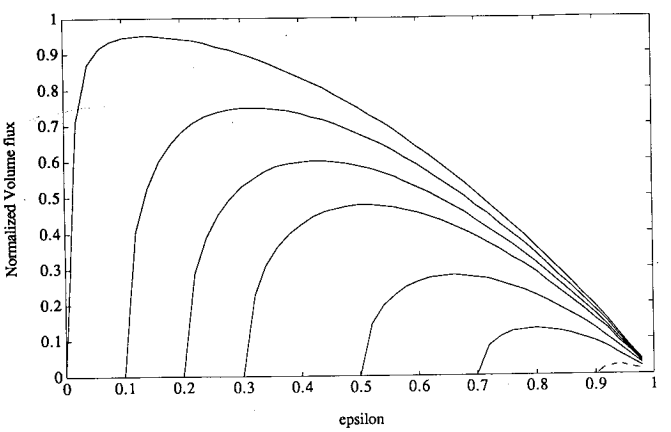

Figure 6 Normalized volume flux Q' versus ε_i for seven values of α_i^2 equivalent to the values of α^2 in Figure 4.

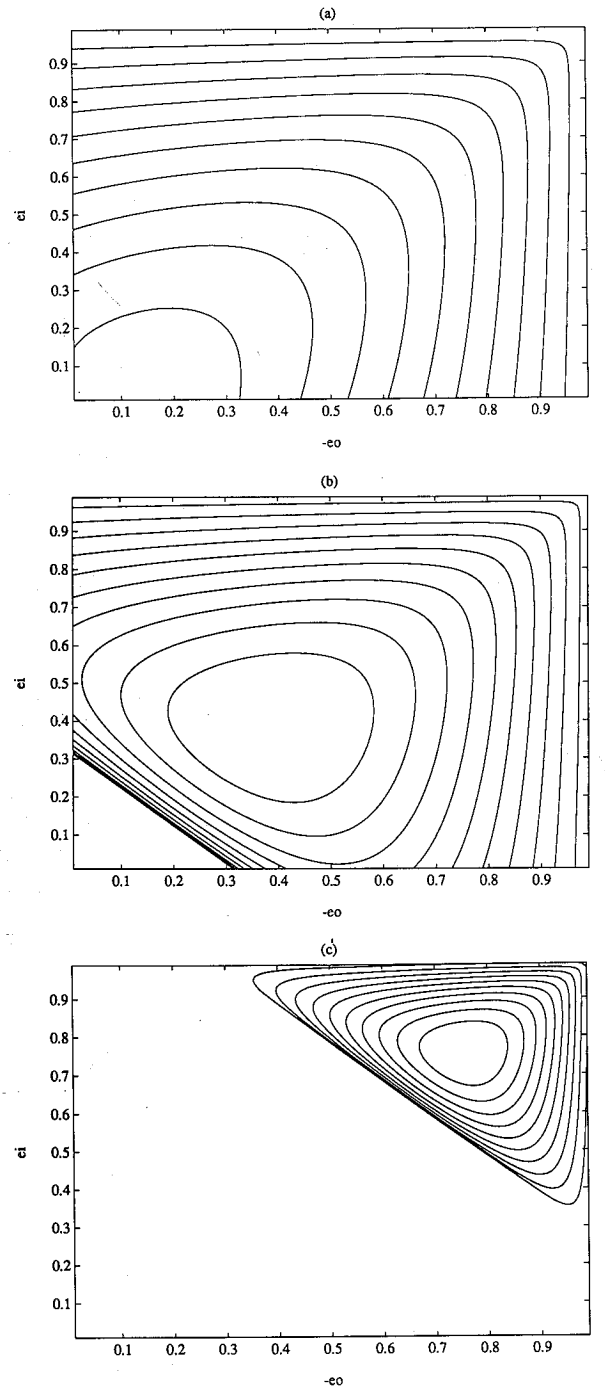

Figure 7 Contours of values (equally spaced) of volume flux as a function of $-\varepsilon_o$ (labeled $-$eo) and e_i (labeled *ei*) for $\gamma = 1.01$. Values of α_r are left to right 0, 40 and 80. Values of maximum flux are 1.007, 0.65 and 0.17, respectively. The contours for $\alpha_r = 0$ are identical to contours calculated for $\alpha_r = 0.1$.

For $\gamma = 1.1$ and 2.0 the results are very similar to the Cartesian ($\gamma = 1.0$) case except that $\varepsilon_i \neq -\varepsilon_o$. However, for $\gamma = 100$ there is the curious result that $F > 1$. This means that flux is greater than the maximum flux that one would calculate for the Cartesian case using the inner radius to calculate the cross section area of the slot. Using the inner radius is quite reasonable since it is well established (Wood 1968) that flux is determined by the minimum opening width. Figure 8 shows that maximum flux is found at very small values of ε_i and appears to exist at moderate values of ε_o but exactly at what value cannot be seen in that figure. The limit for very small values of ε_i is shown in Figure 9, which was obtained by setting ε_i to the constant values of 0, 10^{-5}, and 2×10^{-5}, respectively and varying ε_o between 0.01 and 0.99. There is a singularity when both are zero. It is quite clear that Q' approaches 100, which is the value of γ.

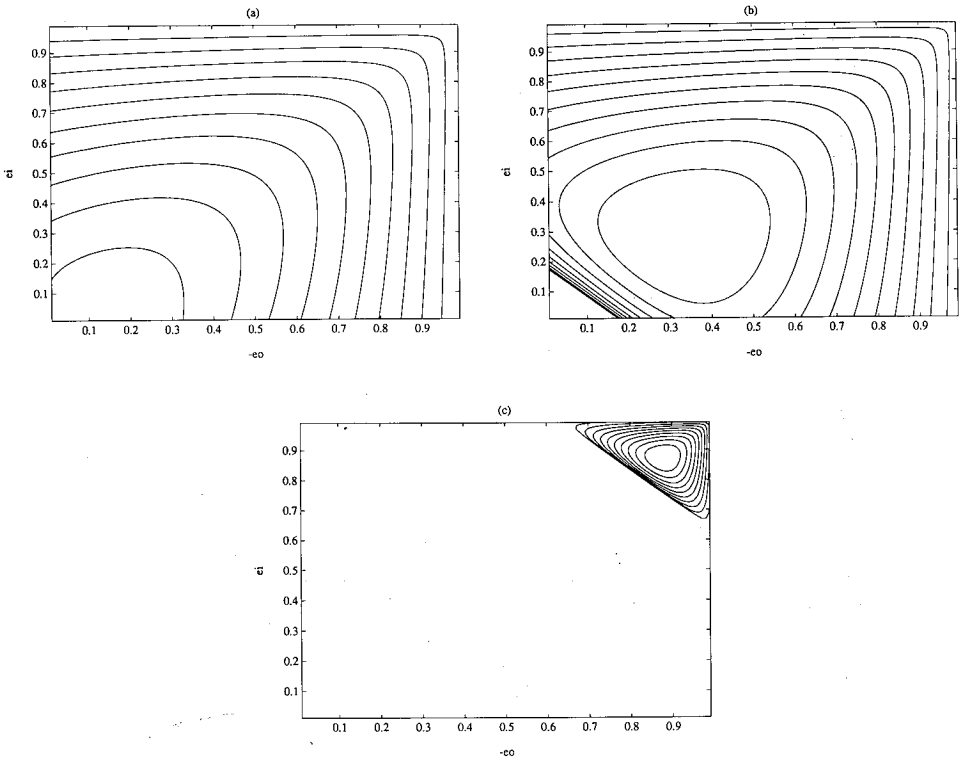

Figure 8 Contours of values (equally spaced) of volume flux as a function of $-\varepsilon_o$ (labeled $-e_o$) and e_i (labeled *ei*) for three values of γ and assorted α_r. The dimensionless cylindrical parameter γ increases downward and the rotation parameter α_r increases left to right. In (a)–(c) $\gamma = 1.1$ and $\alpha_r = 0.1$, 3.0, and 9.0. The maximum values of flux are 1.08, 0.8, and 0.06, respectively. The results are close to those of the Cartesian geometry. In (d)–(f) $\gamma = 2.0$ and $\alpha_r = 0.05$, 0.3, and 0.7. The maximum values of flux are 1.78, 1.06, and 0.18, respectively. The results differ noticeably from the Cartesian results. Notably, the maximum does not happen for $\varepsilon_i = -\varepsilon_o$ for small α_r. In (g)–(i), $\gamma = 100$ so the cylindrical geometry is very pronounced and $\alpha = 0$, 0.0002, and 0.00025. For small rotation maximum flux is 8.80 and is found for small ε_o. A closer examination of the $\varepsilon_o = 0$ axis is shown in the next figure. For moderate rotation maximum flux is 0.84 and is found for ε_i of order one and ε_o small. For rapid rotation maximum flux is 0.21 and is found for $\varepsilon_o > \varepsilon_i$ where both are of order one.

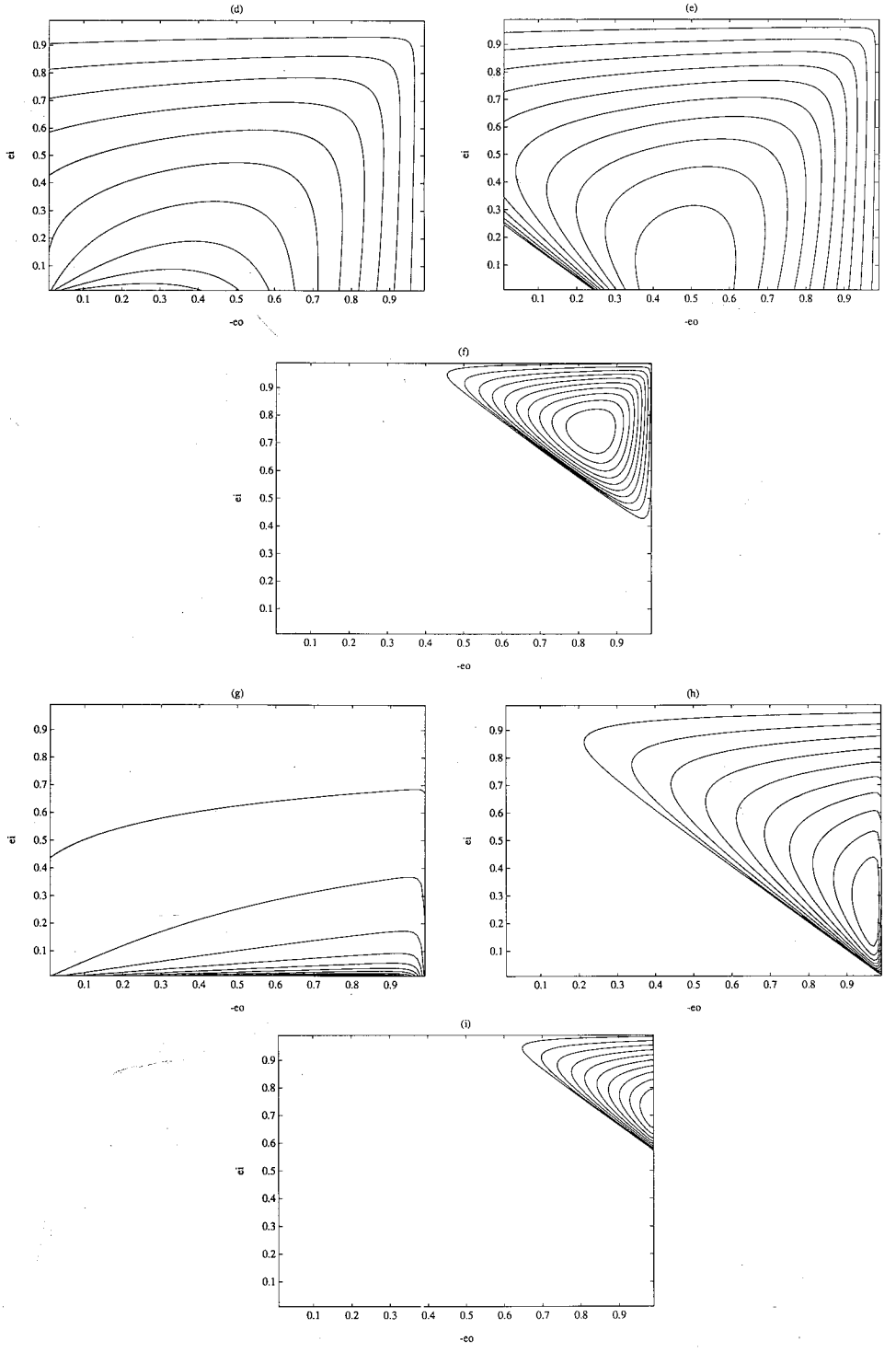

Figure 8 (*Continued.*)

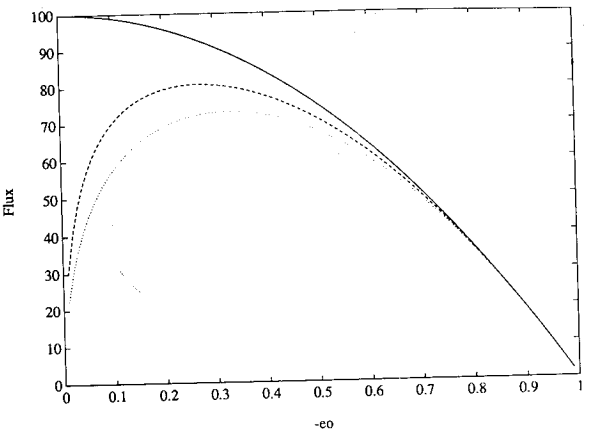

Figure 9 Normalized volume flux Q' versus ε_o for $\varepsilon_i = 0$, (solid), 10^{-5} (dashed), and 2×10^{-5} (dotted) in the pronounced cylindrical geometry $\gamma = 100$ and without rotation ($\alpha_r = 0$). Flux equals γ in the limit $\varepsilon_i = \varepsilon_o = 0$, but departs significantly from that value for small changes in ε_i or ε_o.

To analytically clarify what is happening in this limit, we investigate the results for large γ with $\alpha_r = 0$ in (39). For $1 \gg \varepsilon_o \gg \varepsilon_i$ using $\varepsilon_i = -\beta\varepsilon_o$, it simplifies to

$$F = \frac{2\pi r_o}{4}\sqrt{g'h^3}\left[\frac{1+\beta}{1+\gamma^2\beta}\right]. \tag{40}$$

The function in brackets is maximum at $\beta = 0$ and has a negative slope of $1-\gamma^2$ so F is greatest at $\varepsilon_i = 0$. Now setting $\varepsilon_i = 0$, ($\beta = 0$) in (39) with $\alpha = 0$ but allowing ε_o to vary, we get

$$F = \frac{2\pi r_o}{4}\sqrt{g'h^3}(1-\varepsilon_o^2), \tag{41}$$

which is greatest at $\varepsilon_o = 0$. This can also be found from (38) without invoking large γ. Thus the value of F for (40) with $\beta = 0$ or in (41) with $\varepsilon_o = 0$ is a local maximum. The contours in Figure 8 showed no other maximum, so the maximum at $\varepsilon_i = \varepsilon_o = 0$ appears to be a global maximum. This value of volume flux is puzzling. It is the value of volume flux for a two layer Cartesian solution for the widest part of the opening (of radius r_0) rather than the narrowest part of the opening (of radius r_i). This surprising result is in contrast to other two-layer problems where the *minimum* cross-section area determines the maximum volume flux that can be achieved. Perhaps this is related to the supercritical solution branch shown in Figure 3a.

To investigate the effects of rotation, the values of α in Figure 8 were selected to show specific aspects of the solutions from the weakly rotating, through the moderate and strongly rotating limits. For all three values of γ the manner in which rotational effects come in as α_r is increased resembles that shown in Figure 7. As α_r increases from zero, flux decreases most at small values of ε_i and ε_o which are the values that also produce

maximum flux. As α_r is increased some more zero flux happens first at $\varepsilon_i = \varepsilon_o = 0$. As α_r further increases maximum flux is found at progressively larger values of ε_i (which in addition approaches $-\varepsilon_o$). For sufficiently large α_r the parameters of maximum flux approach $\varepsilon_i = -\varepsilon_o = 1$. In this limit αr^2 approaches the limit $8\gamma^2/(1-\gamma^2)(1-\gamma^4)$ which for large γ is $8\gamma^{-4}$ (a number much less than 1) and maximum flux becomes very small. For still greater α_r, flux becomes zero for all ε. In dimensional units this happens when $r_0 - r_i = 2\sqrt{2}\gamma R/(1+\gamma)\sqrt{1+\gamma^2}$.

In summary, the axisymmetric problem contains many features found in the Cartesian problem, but it also contains some surprising results. For small rotation the values of maximum volume flux and fluid depths at the inner and outer radii are close to those for zero rotation. For greater values of rotation, flux decreases and fluid depths at the inner and outer radii get small. Above a certain rate of rotation no flux is possible, as was true in the Cartesian case. An unexpected result is that maximum volume flux for no rotation and large γ is determined by the width based on outer radius rather than inner radius. This has no simple explanation to date.

4. LABORATORY OBSERVATIONS OF THE RELATION BETWEEN TEMPERATURE DIFFERENCE AND HEAT FLUX

A lock-exchange experiment driven by heat flux was constructed to test the preceding theories. It was hoped to check the predictions for volume flux versus rotation rate and observe the interface shape and fluid depth near the edge of the openings. It was also important to investigate the possibility of instability of these flows. The apparatus (Figure 10) consisted of a square water tank $60 \times 60\,\text{cm}^2$ that was filled with water 30 cm deep. A cylindrical plastic chamber with a flat annular rim was inverted and

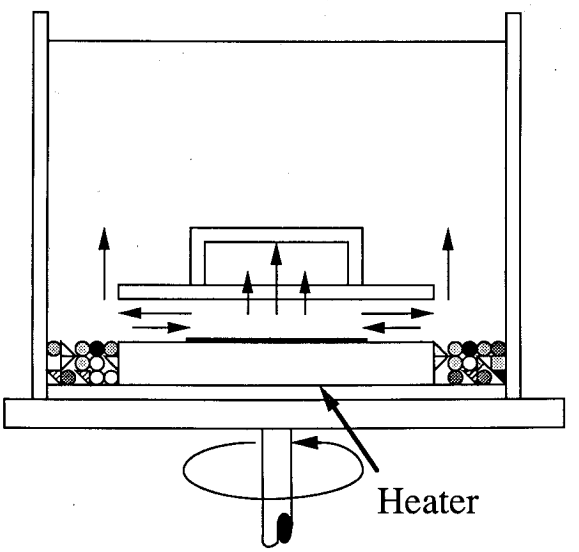

Figure 10 Sketch of the experimental apparatus.

suspended 5 cm above the flat bottom so that the annular rim was horizontal. The inner radius of the rim was 15 cm. Inside this radius was a cylindrical chamber with a top 5 cm above the lower edge of the rim. The outer radius of the rim was 20 cm. On the bottom of the tank, but centered under the plastic chamber and rim was a flat horizontal disk of 20 cm. radius elevated 2 cm above the bottom of the tank. Centered on it was a waterproof electrical heating pad of 15 cm radius. The idea was that after steady voltage was applied to the heater, warm water would rise in convection cells and spread out in the chamber above the heater. Once that was filled with warm water, the heated water would flow outward under the rim until it passed to the outer edge of the rim. Then it would rise to the top of the tank and pass out of the area of interest. To replace this outflow, cold water at the bottom of the tank would flow inward until it passed over the heating pad. Once there it would be heated from below, acquire convection cells, and complete the flow cycle by rising into the chamber above. To insure that the bottom cold water had no large circulation at a radius greater than 20 cm, small rocks of about 1/2 cm size were piled outside the 20 cm radius of the bottom disc to the depth of its elevation above the bottom—roughly 2 cm. Inward flowing water passing over and through the rocks will be spun up to approximately the tank rotation rate.

Thus there was a lock-exchange flow under the rim. Just above the bottom, cold water flowed inward from beyond a 20 cm radius to the heated region which began at a radius of 15 cm. Above that layer of cold water, but below the rim, was an outward flowing layer of warm water. In steady state it is expected that if conductive heat losses through the walls in the inner regions can be neglected, the heat flux of the exchange flow should equal the heating rate of the heater.

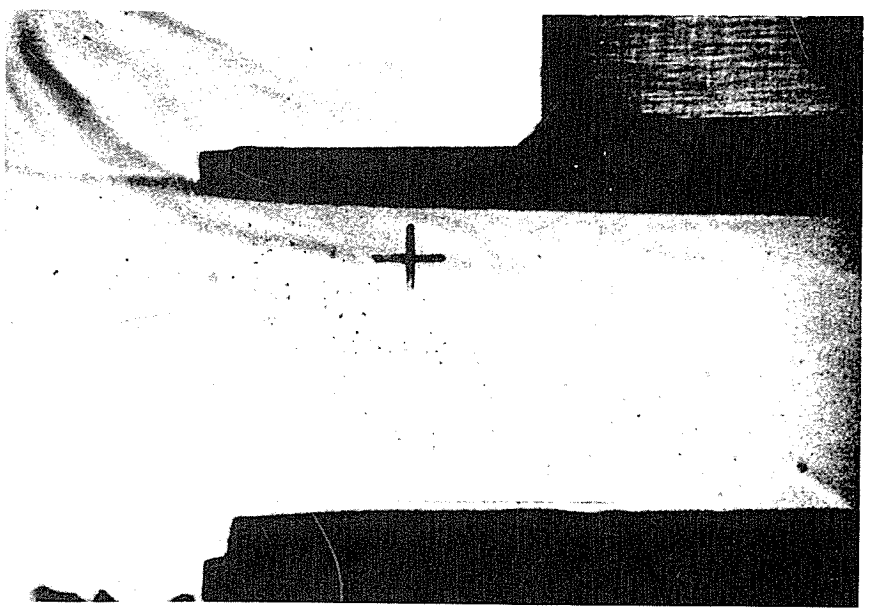

Figure 11 Shadowgraphs of the interface in the axisymmetric geometry ($\gamma = 1.33$) for zero rotation (top) and $f = 0.4\ s^{-1}$ (bottom).

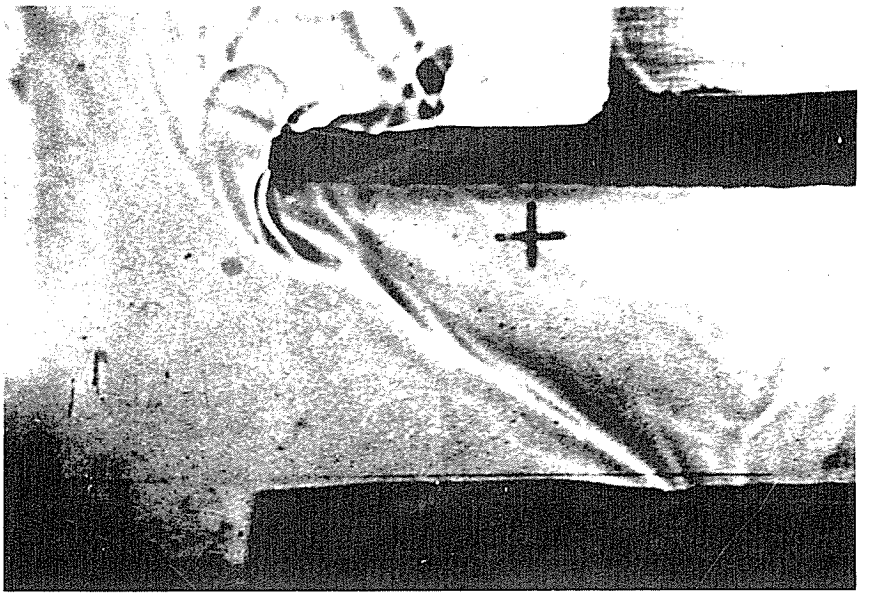

Figure 11 (*Continued.*)

A photograph of the interface was obtained using shadowgraph. Light from a distant slide projector was beamed horizontally through the sides of the tank and onto frosted mylar attached to the side of the tank. Once each revolution the beam would line up with the screen so a shadowgraph would be viewed. A shadowgraph has bright regions from maxima in the second derivative of the density field that signify fronts. Photographs are shown for zero rotation and $f = -0.4\,s^{-1}$ (Figure 11). It is expected from the Cartesian theory that the interface would stay flat midway between the two plates for zero rotation (i.e. ε at r_i and r_o stays close to 0). This does not seem to be the case in detail, and ε seems to be closer to 1/2 at r_i and r_o. The rotating case does seem to possess large ε at r_i at r_o since the layer depths seems to be relatively small. This agrees with the theory.

Measurements of temperature difference between the outflowing and inflowing water were taken for a fixed heater voltage of 69.0 volts (rms). Since the heating pad had an electrical resistance of 12.0 ohms, this voltage produced 397 watts of heat flux. Two thermistors were used to measure the temperature of the warm water. One thermistor was located at a level 1 or 2 mm above the level of the rim in the cavity. The other was located under the rim at a radius of 16 cm, and about 3 mm below the level of the rim. A third thermistor recorded the temperature of the cold inflowing water. It was at approximately 21 cm radius from the center and touched the bottom of the tank.

The temperature differences between the two thermistors in the hot water and the thermistor in the cold water are shown for fourteen different rotation rates in Figure 12. There is a systematic increase in temperature difference with rotation. There is not precise quantitative agreement with a formula based on

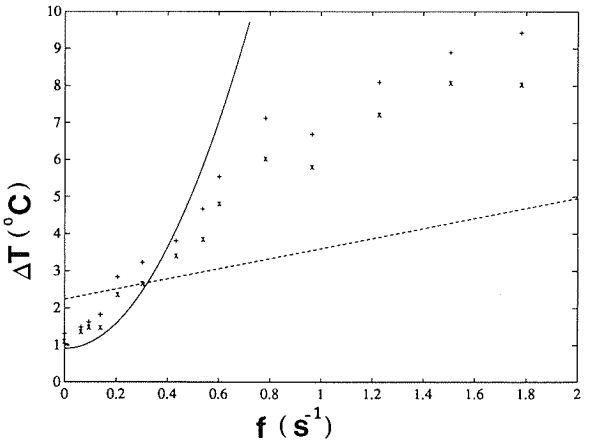

Figure 12 Measurement of temperature difference versus rotation rate for constant heating. The solid curve comes from equation (44). The dashed curve is an empirical formula from the experiment in Whitehead (1993).

the lock-exchange theory. To find this out, equation (25) was used along with the volume flux scale given after equation (17) and the relation between volume flux and heat flux H

$$H = 2\pi r_i \rho C_p \Delta T Q. \tag{42}$$

This gives

$$\Delta T = \frac{1}{g\lambda h}\left[3\left(\frac{g\lambda H}{2\pi r_i \rho C_p}\right)^{2/3} + f^2 l^2\right], \tag{43}$$

where λ is coefficient of thermal expansion, C_p is specific heat, H is heat flux, and r_i is the inner radius. This equation is not precisely correct as f approaches zero. It predicts about 20% larger temperature difference than the correct zero rotation solution given by equation (23) with $\alpha = 0$. In addition, it comes from the Cartesian solution although the experiment is axisymmetric. But, for this value of radii ratio (less than $\gamma = 2$) there is little difference. Therefore for a crude comparison with data, it is useful to have a formula as simple as this. Using values $\rho C_p = 4.18 \times 10^6 \,\mathrm{j\,m^{-3}\,°C^{-1}}$, $g = 9.8\,\mathrm{m\,s^{-2}}$, $\lambda = 3 \times 10^{-4}\,\mathrm{°C^{-1}}$, $l = 0.05\,\mathrm{m}$, $h = 0.05\,\mathrm{m}$, and $r = 0.15\,\mathrm{m}$, the formula becomes

$$\Delta T = 0.91 + 17.0 f^2\,\mathrm{°C}. \tag{44}$$

This curve is also plotted as the solid curve in Figure 12. Predicted temperature difference ΔT is a little lower than the measured data in the region near zero rotation (probably because the fluid is gradually warming and transient effects have been neglected). As rotation increases, the measured temperature difference increases in parallel with the prediction curve. However, at roughly $f = 0.4\,\mathrm{s^{-1}}$ the predicted

temperature difference starts increasing with f much more strongly than the data so that for $f > 1.0\,\mathrm{s}^{-1}$ disagreement is more than a factor of two.

Inspection of the recording of temperature with time reveals that there is a transition to a flow with eddies as rotation is increased. These eddies have been seen both by using dye visualization of the flow and with a time series of the temperature record. This transition apparently increases the heat flux to a value above the rotating lock-exchange prediction. The eddies probably come from baroclinic or barotropic instability. The possibility of developing baroclinic instability is estimated here using the results of Barcilon (1964). He showed in his Figure 4 that instability in a heated annular channel with $\gamma = 3$ may develop if the slope of the isotherms (in that notation $\Delta T_H/\Delta T_v) > \sqrt{200\,Ek}$. Here Ek is the Ekman number $\nu/f(r_o - r_i)^2$, where ν is kinematic viscosity. In our experiment, $\nu = 0.01\,\mathrm{cm}^2/\mathrm{s}$ so that $f = 0.4\,\mathrm{s}^{-1}$ the quantity $\sqrt{200\,Ek} = 0.45$. If the interface slope is greater than roughly 1/2 this criterion is met. In addition, his parameter β (which is equal to our $1/\alpha^2$) must be less than approximately 0.6. This means that $R < \sqrt{0.6}$ times the difference of radii $r_o - r_i = 4\,\mathrm{cm}$. In our experiment for $f = 0.4\ \mathrm{s}^{-1}$, the value of ΔT is approximately 4°C. Using the above formulas for R and a coefficient of expansion for water as given before, R is 2.75 cm and it appears that R at this value of f is just small enough to fit this instability criterion (although just barely so). For the experiments with larger f the instability criterion is clearly exceeded and instability should be present.

Finally, the empiracle curve for a recent experiment with a large laboratory model (Whitehead 1993) of a cooling continental shelf is included in Figure 12. The data are close to the same value of the curve at low rotation rates but they diverge at larger rotation rates. Since that curve is believed to include some effects of thermal conduction, the divergence is expected.

5. SUMMARY

The results for the Cartesian case are not surprising. Volume flux decreases as rotation increases (hence R decreases) and flux goes to zero when R equals slot length. However as that length is approached, both crude estimates and laboratory observations indicate that baroclinic instability develops. The laboratory experiments indicate that the instability allows more heat (and probably volume) flux. It may not be difficult to produce a theory of flux of the baroclinic waves since the conserved properties of the flow are known, but such a theory has not been developed here nor has it been produced elsewhere.

For the case of a cylindrical geometry flux decreases to zero when the difference between radii equals $2\sqrt{2}\gamma R/(1+\gamma)\sqrt{1+\gamma^2}$. This may be important for eddies or cyclones in the ocean or atmosphere. When the outer radius is smaller than R, the flow appears to take the form of a stable, stationary eddy that can have very strong swirl at even relatively small rates of rotation if the inner radius is small. Our results indicate that in that case there will be radial flux of fluid. For conservative (adiabatic, dry, frictionless, etc.) eddies, this would cause the eddy to gravitationally slump until it approached the Rossby Radius. However, if there is some departure from conservative

motions, this slumping may be impeded and the radial flux may continue indefinitely. Such an effect may happen in cyclones, in which case the present considerations may have some bearing since the Ekman layer is not required to be an agent of the inward flow as in the usual picture of the CISK (conditional instability of the second kind (Charney and Elliassen, 1964; Emanuel, 1991; Yoshimoto and Kimura, 1993) instability.

At slow rotation rate the lock-exchange experiment driven by electrical heating produced temperature difference measurements for given heat flux and rotation that had the correct order of magnitude as the theory for slow rotation but differed in detail by tens of percent. There was poor agreement above a critical rotation rate where a transition to a flow with eddies (probably from baroclinic instability) shows evidence of increased heat flux.

Acknowledgements

Stimulation for this joint work was provided by the program "Study on water exchange processes across the shelf edge" organized by Professor Sugimoto, Ocean Research Institute, University of Tokyo with Grant-in-Aid by the Japanese Government under grant number 03045018 which supported visits of the investigators to each other's institution during the past two years. Support for the research of J.W. on laboratory studies of fronts on shelves is provided by the Coastal Sciences Section, Code 321 CS of the Office of Naval Research, under grant number N00014-89-J-1037. We thank Steve Lentz for useful suggestions. Woods Hole Oceanographic Institution Contribution number 8609.

References

Barcilon, V., "Thermally driven motion of a stably stratified fluid in a rotating annulus," *Ph. D. Thesis*, Harvard University, (1962).

Barcilon, V., "The role of Ekman layers in the stability of the symmetric regime obtained in a rotating annulus," *J. Atmos. Sci.* **21**, 291–299 (1964).

Bowden, M. and Eden, H. F., "Thermal convection in a rotating fluid annulus: temperature, heat flow and flow field observations in the upper symmetric regime," *J. Atmos. Sci.* **22**, 185–195 (1965).

Chao, Shenn-Yu., "Instabilities of fronts over a continental margin," *J. Geophys. Res.* **95**, **C3**, No. C3, 3199–3211 (1990).

Charney, J. and Elliassen, A., "On the growth of the hurricane depression," *J. Atmos. Sci.* **21**, 68–75 (1964).

Csanady, G. T., "The influence of wind stress and river runoff on a shelf-sea front," *J. Phys. Oceanogr.* **14**, 1383–1392 (1984).

Emanuel, K., "The theory of hurricanes," *Ann. Rev. Fluid Mech.* **23**, 179–196 (1991).

Flagg, C. N. and Beardsley, R. C., "On the stability of the shelf water/slope water front south of New England," *J. Geophys. Res.* **83**, **C9**, 4623–4631 (1978).

Fowlis, W. W. and Hide, R., "Thermal convection in a rotating annulus: effect of viscosity on the transition between axisymmetric and non-axisymmetric flow regimes," *J. Atmos. Sci.* **22**, 541–558 (1965).

Gawarkiewicz, G., "Linear stability models of Shelfbreak fronts", *J. Phys. Oceanogr.* **21**, 471–488 (1991).

Gawarkiewicz, G. and Chapman, D. C., "The role of stratification in the formation and maintenance of shelf-break fronts," *J. Phys. Oceanogr.* **22**, 753–771 (1992).

Hignett, P., Ibbetson, A. and Killworth, P., "On rotating thermal convection driven by non-unform heating from below," *J. Fluid Mech.* **109**, 161–187 (1981).

Robinson, A. R., "The symmetric state of a rotating fluid differentially heated in the horizontal," *J. Fluid. Mech.* **6**, 599–620 (1959).

Sambuco, E. and Whitehead, J. A. Jr., "Hydraulic control by a wide weir in a rotating fluid," *J. Fluid Mech.* **73**, 521–528 (1976).

Stommel, H. and Leetmaa, A., "The circulation on the continental shelf," *Proc. Natl. Acad. Sci.* **69**, 3380–3384 (1972).

Vincent, C. L., Royer, T. C. and Brink, K. H., "Long time series measurements in the coastal ocean: A workshop", Woods Hole Oceanographic Institution Technical Report WHOI-93-49 (1993).

Walsh, J. J., Biscaye, P. E. and Csanady, G. T., "The 1983–1984 shelf edge exchange processes (SEEP)-I Experiment: Hypothesis and highlights. *Cont. Shelf Res.* **8**, 435–456 (1988).

Whitehead, J. A., "A laboratory model of cooling over the continental shelf," *J. Phys. Oceanogr.* **23** (11), 2412–2427 (1993).

Whitehead, J. A. and Porter, D. L., "Axisymmetric critical withdrawal of a rotating fluid," *Dyn. Ocns. Atm.* **2**, 1–18 (1977).

Wood, I. R., "A lock-exchange flow," *J. Fluid Mech.* **42**, 671–687 (1970).

Yih, C. S., *'Stratified flows*, Academic Press, San Diego CA (1980).

Yoshimoto, M. and Kimura, R., "A source-sink vortex as a hydrodynamic model of tropical cyclone," *Fluid Dyn. Res.* **11**, 171–181 (1993).

GEOPHYSICAL AND ASTROPHYSICAL FLUID DYNAMICS

AIMS AND SCOPE

Geophysical and Astrophysical Fluid Dynamics exists for the publication of original research papers and short communications, occasional survey articles and conference reports on the fluid mechanics of the earth and planets, including oceans, atmospheres and interiors, and the fluid mechanics of the sun, stars and other astrophysical objects. In addition, their magnetohydrodynamic behaviors are investigated. Experimental, theoretical and numerical studies of rotating, stratified and converging fluids of general interest to geophysicists and astrophysicists appear. Properly interpreted observational results are also published.

Notes for contributors can be found at the back of the journal.

Ordering Information
Four issues per volume. 1994 Volumes: 75-79.
Orders may be placed with your usual supplier or directly with Gordon and Breach Science Publishers SA in care of the addresses shown on the inside back cover. Journal subscriptions are sold on a per volume basis only; single issues of the current volume are not available separately. Claims for nonreceipt of issues will be honored free of charge if made within three months of publication of the issue. Subscriptions are available for microform editions; details will be furnished upon request.

All issues are dispatched by airmail throughout the world.

Subscription Rates
Base list subscription price per volume: ECU 266.00 (US $290.00)*. This price is available only to individuals whose library subscribes to the journal OR who warrant that the journal is for their own use and provide a home address for mailing. Orders must be sent directly to the Publisher and payment must be made by personal check or credit card.

(continued on inside back cover)